EUROPEAN ORGANIZATION FOR NUCLEAR RESEARCH

CERN-PPE/92-100
June 19, 1992

A Measurement of Single and Double Prompt Photon Production at the CERN $\overline{p}p$ Collider

The UA2 Collaboration

Bern - Cambridge - CERN - Dortmund - Heidelberg - Melbourne -
Milano - Orsay (LAL) - Pavia - Perugia - Pisa - Saclay (CEN)

J. Alitti[12], G. Ambrosini[9], R. Ansari[8], D. Autiero[11], P. Bareyre[12], I. A. Bertram[6], G. Blaylock[3,a], P. Bonamy[12], K. Borer[1], M. Bourliaud[12], D. Buskulic[8], G. Carboni[11], D. Cavalli[7], V. Cavasinni[11], P. Cenci[10], J. C. Chollet[8], C. Conta[9], G. Costa[7], F. Costantini[11], L. Cozzi[7], A. Cravero[7], M. Curatolo[11], A. Dell'Acqua[3,9], T. DelPrete[11], R. S. DeWolf[2], L. DiLella[3], Y. Ducros[12], G. F. Egan[6], K. F. Einsweiler[3,b], B. Esposito[11], L. Fayard[8], A. Federspiel[1], R. Ferrari[9], M. Fraternali[9], D. Froidevaux[3], G. Fumagalli[9], J. M. Gaillard[8,3], F. Gianotti[7], O. Gildemeister[3], C. Gössling[4], V. G. Goggi[9], S. Grünendahl[5], K. Hara[1,c], S. Hellman[3], J. Hřivnáč[3,d], H. Hufnagel[4], E. Hugentobler[1], K. Hultqvist[3,e], E. Iacopini[11,f], J. Incandela[7,g], K. Jakobs[3,h], P. Jenni[3], E. E. Kluge[5], N. Kurz[5], S. Lami[11], P. Lariccia[10], M. Lefebvre[3,i], L. Linssen[3], M. Livan[9], P. Lubrano[3,10], C. Magneville[12], L. Malgeri[j], L. Mandelli[7], L. Mapelli[3], M. Mazzanti[7], K. Meier[3,k], B. Merkel[8], J. P. Meyer[12], M. Moniez[8], R. Moning[1], M. Morganti[11], L. Müller[1], D. J. Munday[2], M. Nessi[3], F. Nessi-Tedaldi[3,l], C. Onions[3], T. Pal[1,m], M. A. Parker[2], G. Parrour[8], F. Pastore[9], E. Pennacchio[9], J. M. Pentney[3,n], M. Pepe[3], L. Perini[7], C. Petridou[11,o], P. Petroff[8], H. Plothow-Besch[3], G. Polesello[3,9], A. Poppleton[3], K. Pretzl[1], M. Primavera[11,j], M. Punturo[10], J. P. Repellin[8], A. Rimoldi[9], M. Sacchi[9], P. Scampoli[10], J. Schacher[1], B. Schmidt[4], V. Šimák[3,d], S. L. Singh[2], V. Sondermann[4], R. Spiwoks[4], S. Stapnes[3,p], C. Talamonti[10], F. Tondini[10], S. N. Tovey[6], E. Tsesmelis[4], G. Unal[8], M. Valdata-Nappi[11,j], V. Vercesi[9], A. R. Weidberg[3,q], P. S. Wells[2,r], T. O. White[2], D. R. Wood[8,g], S. A. Wotton[2,r], H. Zaccone[12], A. Zylberstejn[12]

(Submitted to Phys. Lett. B)

Abstract

A measurement of the cross sections for single and double prompt photon production in $\bar{p}p$ interactions at $\sqrt{s} = 630$ GeV is presented. The data sample corresponds to an integrated luminosity of 13.2 pb^{-1}. The results are in good agreement with the predictions of perturbative QCD. The signal from double prompt photon production has a statistical significance of 4.3 standard deviations.

[1]Laboratorium für Hochenergiephysik, Universität Bern, Sidlerstraße 5, 3012 Bern, Switzerland
[2]Cavendish Laboratory, University of Cambridge, Cambridge, CB3 0HE, UK
[3]CERN, 1211 Geneva 23, Switzerland
[4]Lehrstuhl für Exp. Physik IV, Universität Dortmund, 4600 Dortmund, FRG
[5]Institut für Hochenergiephysik der Universität Heidelberg, Schröderstraße 90, 6900 Heidelberg, FRG
[6]School of Physics, University of Melbourne, Parkville 3052, Australia
[7]Dipartimento di Fisica dell'Università di Milano and Sezione INFN Milano, 20133 Milano, Italy
[8]Laboratoire de l'Accélérateur Linéaire, Université de Paris-Sud, 91405 Orsay, France
[9]Dipartimento di Fisica Nucleare e Teorica, Università di Pavia and INFN, Sezione di Pavia, Via Bassi 6, Pavia, Italy
[10]Dipartimento di Fisica dell'Università di Perugia and INFN, Sezione di Perugia, Via Pascoli, 06100 Perugia, Italy
[11]Dipartimento di Fisica dell'Università di Pisa and INFN Sezione di Pisa, Via Livornese, S. Piero a Grado, 56100 Pisa, Italy
[12]Centre d'Etudes Nucléaires de Saclay, 91191 Gif-sur-Yvette Cedex, France
a) Now at University of California, Santa Cruz, USA
b) Now at Lawrence Berkeley Laboratory, Berkeley, California, USA
c) Now at University of Tsukuba, Tsukuba, Ibaraki 305, Japan
d) Now at Institute of Physics, CSAV, Na Slovance 2, Praha 8, Czechoslovakia
e) Now at University of Stockholm, Stockholm, Sweden
f) Also at Scuola Normale Superiore, Pisa, Italy
g) Now at FNAL, Batavia, USA
h) Now at Max Planck Institut für Physik, Föhringer Ring, D-8000 München, FRG
i) Now at University of Victoria, Victoria, Canada
j) Now at Dipartimento di Fisica dell'Università della Calabria e gruppo INFN, Cosenza, Italy
k) Now at Deutsches Elektronen Synchrotron, Hamburg, FRG
l) Now at Eidgenössische Technische Hochschule, ETH Zürich, CH-8093 Zürich, Switzerland
m) Now at SSCL, 2550 Beckleymeade Av., Dallas, Texas, USA
n) Now at Department of Physics, Brunel University, Uxbridge, London, UK
o) Now at INFN Sezione di Trieste, Laboratori-Area di Ricerca, Padriciano 99, 34012 Trieste, Italy
p) Now at Physics Institute, Univerity of Oslo, Blindern, Oslo, Norway
q) Now at Nuclear Physics Laboratory, University of Oxford, Oxford, UK
r) Now at CERN, Geneva, Switzerland

1 Introduction

The study of the production of large transverse momentum (p_T) photons in hadron–hadron collisions is a convenient way to extract information about the constituents of hadronic matter and their interactions. A measurement of the direct photon cross–section provides a test of QCD with the advantage that the photon transverse momentum is not affected by fragmentation effects, resulting in experimental uncertainties which are considerably smaller than those obtained, for instance, in the measurement of a jet cross–section. Next–to–leading order calculations both for single and double prompt photon production are available [1]–[3] and can be directly compared to the experimental results.

The main source of background to the photon signal is the production of high transverse momentum hadron jets since they often contain one or more π^0 (or η) mesons which decay into photon pairs that cannot be resolved at high energy. For both single and double prompt photon production, this background is overwhelming, due to the low production cross–section of prompt photon processes with respect to jet production. Prompt photon production, however, results in isolated electromagnetic clusters, whereas the background from hadron jets is accompanied by jet fragments, so that an "isolation requirement" is very effective in reducing the background in the signal sample.

An additional difficulty for the study of double prompt photon production is the very low cross–section, of the order of a few picobarns for the p_T range explored by collider experiments, requiring a high statistics sample for the extraction of a meaningful signal.

Using the integrated luminosity of 13.2 pb^{-1} accumulated during the 1988–90 UA2 runs, a measurement of the single prompt photon production cross–section was performed with higher statistics than previous measurements [4, 5]. Furthermore a signal from double prompt photon production was observed with a statistical significance of 4.3 standard deviations.

2 The UA2 Apparatus

The upgraded UA2 detector [6] provides full azimuthal coverage around the interaction region in the pseudorapidity range $-3 < \eta < 3$ and consists of a central tracking detector surrounded by electromagnetic and hadronic calorimeters [7].

The calorimeter is divided into a central part (CC) with $\mid \eta \mid < 1$ and two end cap regions (EC) reaching $\mid \eta \mid = 3$. All calorimeters use the sampling technique, with a tower structure and wavelength shifter readout. The granularity is $\Delta\theta \cdot \Delta\phi = 10° \cdot 15°$ in the CC and $\Delta\eta \cdot \Delta\phi = 0.2 \cdot 15°$ in the EC, except for the two cells closest to the beam axis where $\Delta\eta = 0.3$ and 0.5 respectively. The electromagnetic compartments are multi–layer lead–scintillator sandwiches with a total thickness of 17 radiation lengths (r.l.) in the CC and varying between 17.1 and 24.4 r.l. in the EC, depending on the polar angle θ. The hadronic compartments are multi–layer iron–scintillator sandwiches, 4 absorption lengths (a.l.) deep in the CC and 6.5 a.l. deep in the EC.

The central detector, used to determine the position of the event vertex and to reconstruct charged particle tracks, consists of two silicon pad counter arrays [8] around

the beam at radii of 2.9 cm and 14.8 cm. A cylindrical drift chamber [9] is located between the two silicon detectors. Beyond the outer silicon layer there is a transition radiation detector [10], consisting of two sets of radiators and proportional chambers, followed by a scintillating fibre detector SFD [11] which provides track segments in the first six stereo triplets of fibres and localizes the beginning of electromagnetic showers in front of the CC in the last two stereo triplets, located after a 1.5 r.l. thick lead converter.

In the forward regions, $\mid \eta \mid > 1$, tracking and preshower measurements are provided by three stereo triplets of proportional tubes [12] placed in front of the end cap calorimeters. The first two triplets are used as a tracking device, while the last triplet, placed after a 2 r.l. thick iron and lead converter, acts as a preshower detector. Two sets of time–of–flight hodoscopes are located at small angles with respect to the beam. Their function is to define a minimum bias trigger and to provide an independent vertex measurement. Finally, two planes of large area scintillation counters cover the back sides of the end cap calorimeters. Events caused by beam halo particles are rejected in the analysis by detecting charged particles giving an early signal in these counters with respect to the beam crossing time.

3 Photon selection and background subtraction

The events are selected by requiring a reconstructed vertex within a distance along the beam line smaller than 250 mm from the detector centre, and the presence of one or two electromagnetic clusters. Clustering is performed in the calorimeter by joining all cells with an energy greater than 400 MeV sharing a common edge. Clusters with a small lateral size and a small energy leakage into the hadronic compartments are marked as electromagnetic. A photon candidate is defined as an electromagnetic cluster satisfying the following criteria :

- Lateral and longitudinal profiles of the cluster consistent with that expected for a single isolated electron or photon.
- The absence of charged tracks in front of the calorimeter cluster, ensured by pulse height cuts on any silicon pads present in either silicon counter within a window of $\Delta\eta < 0.2$ and $\Delta\phi < 15°$ about the cluster axis (defined by the line joining the interaction vertex to the cluster centroid).
- At most, one preshower signal in a cone $\sqrt{\Delta\phi^2 + \Delta\eta^2} < 0.265$ about the cluster axis.

The applied isolation criteria reject a large fraction of π^0's and η's at the same time mantaining a high efficiency for direct photons. The residual background contamination is measured and subtracted on a statistical basis, by considering the fraction α of photons in the sample that initiate showers in the converter of the preshower detector. A converted photon candidate is defined by the observation of a signal above a threshold of 3 minimum ionizing particle (MIP) equivalents in the preshower detector, otherwise the photon candidate is referred to as unconverted. In order to compute α, all the selection

efficiencies which have a different value for converted and unconverted photon candidates have been taken into account, as discussed in Ref. [5], to determine the true numbers of converted (N_c^{true}) and of unconverted (N_u^{true}) photons from the number of observed photon candidates. The conversion probability α in the sample is then computed as :

$$\alpha = \frac{N_c^{true}}{N_c^{true} + N_u^{true}}$$

The conversion probability ε_γ of an incident single photon is evaluated as a function of the photon energy using the EGS shower simulation programme [13]. The simulation has been tuned to describe correctly the preshower detector response to test beam electrons of 10 and 40 GeV and to electrons from W decays. The total systematic error on ε_γ is estimated to decrease with energy from 2.4% to 2.0% in the energy range between 17 and 90 GeV corresponding to the data sample. The multiphoton conversion probability ε_π for photon pairs produced by single π^0 and η decays is calculated using ε_γ for each photon and assuming that the ratio between the number of η and π^0 is 0.6 and p_T independent [14]. The component of multi-π^0 states in the background has been estimated [5] by comparing the conversion probability measured for a background data sample with the value of ε_π calculated from single π^0's and η's. This component has turned out to be highly suppressed by the preshower isolation requirement. The systematic error on ε_π is mainly due to the uncertainty in the two-photon angular resolving power and ranges from 2.7% to 1.5% with increasing π^0 energy, for energy values between 17 and 90 GeV. The calculated values of ε_π and ε_γ are compared in Fig. 1a with the measured conversion probability α as a function of the cluster energy E_γ . The measured values lie between the two theoretical curves and tend towards ε_γ as E_γ increases.

The fraction of multiphoton events in the sample,

$$b(p_T) \;=\; \frac{\alpha - \varepsilon_\gamma}{\varepsilon_\pi - \varepsilon_\gamma}$$

computed in each p_T-bin is shown in Fig. 1b to decrease with increasing p_T, as expected from Fig. 1a.

4 Single photon inclusive cross-section

The present analysis is based on events selected during the 1988-90 collider runs. The data from the 1988 and 1989 runs were selected using the single electron trigger [15], requiring the presence of an electromagnetic cluster with $p_T > 12$ GeV. This trigger is found to be fully efficient above the offline p_T threshold of 15 GeV. In 1990, in order to cope with the increased peak luminosity, the online p_T threshold, set to 18 GeV, was combined to a requirement of small lateral cluster profile. This trigger is found to be fully efficient for $p_T > 21$ GeV. For this reason the final cross-section has been computed using the 1988-89 data only in the case of photon candidates with p_T between 15 and 21 GeV, and using the full sample for candidates with $p_T > 21$ GeV. Only events with a single reconstructed $\overline{p}p$ interaction vertex and having an electromagnetic cluster well

contained in the fiducial region of the central calorimeter ($|\eta| < 0.76$) are considered. In addition the events must contain at least one cluster with the characteristics expected for an isolated single photon. A total of 21117 photon candidates with $15 < p_T \leq 21$ GeV from the 1988–89 sample and 9017 candidates with $p_T > 21$ GeV from the full 1988–90 data sample is found.

The invariant inclusive cross–section for direct photon production is evaluated from

$$E\frac{d\sigma}{d^3p} = \frac{N_\gamma(p_T)\cdot[1-b(p_T)]}{2\pi\ p_T\ \Delta p_T\ \mathcal{L}\ \varepsilon_c\ A(p_T)}$$

where $N_\gamma(p_T)$ is the number of photon candidates in a p_T–bin of width Δp_T, $b(p_T)$ is the background fraction in that bin, $\mathcal{L} = 13.2 \pm 0.7\ pb^{-1}$ is the integrated luminosity corresponding to the data sample, ε_c is the direct photon detection efficiency and $A(p_T)$ is the geometrical acceptance. The global detection efficiency $\varepsilon_c = 0.454 \pm 0.011$ does not include the effects associated with photon conversions in the preshower detector, which have been taken into account in the calculation of the conversion probability as discussed in section 3.

Table 1: Inclusive direct photon cross–section at $|\eta| = 0$.

$< p_T >\ (GeV)$	$E\frac{d\sigma}{d^3p}\ (pb\ GeV^{-2})$	Uncertainty $(pb\ GeV^{-2})$		
		stat.	syst.	tot.
15.9	7.46	$4.10\ 10^{-1}$	1.41	1.47
17.9	3.97	$2.51\ 10^{-1}$	$6.71\ 10^{-1}$	$7.17\ 10^{-1}$
19.9	1.79	$1.56\ 10^{-1}$	$2.99\ 10^{-1}$	$3.38\ 10^{-1}$
21.9	$9.92\ 10^{-1}$	$7.13\ 10^{-2}$	$1.59\ 10^{-1}$	$1.74\ 10^{-1}$
23.9	$6.15\ 10^{-1}$	$5.00\ 10^{-2}$	$7.93\ 10^{-2}$	$9.38\ 10^{-2}$
25.9	$3.66\ 10^{-1}$	$3.62\ 10^{-2}$	$4.51\ 10^{-2}$	$5.78\ 10^{-2}$
28.7	$1.51\ 10^{-1}$	$1.60\ 10^{-2}$	$1.82\ 10^{-2}$	$2.42\ 10^{-2}$
33.5	$6.57\ 10^{-2}$	$7.28\ 10^{-3}$	$7.69\ 10^{-3}$	$1.06\ 10^{-2}$
38.6	$1.79\ 10^{-2}$	$3.67\ 10^{-3}$	$1.68\ 10^{-3}$	$4.04\ 10^{-3}$
46.3	$6.94\ 10^{-3}$	$1.71\ 10^{-3}$	$7.50\ 10^{-4}$	$1.87\ 10^{-3}$
54.1	$2.31\ 10^{-3}$	$9.36\ 10^{-4}$	$3.49\ 10^{-4}$	$9.99\ 10^{-4}$
64.5	$4.84\ 10^{-4}$	$2.72\ 10^{-4}$	$5.76\ 10^{-5}$	$2.78\ 10^{-4}$
82.3	$1.51\ 10^{-4}$	$9.99\ 10^{-5}$	$1.45\ 10^{-5}$	$1.01\ 10^{-4}$

The remaining background caused by beam halo particles has been estimated to be less than 1% of the photon candidate sample at all p_T and has been neglected. The contribution from $W \rightarrow e\nu$ decays where no electron track was reconstructed is estimated

to be [5] 0.2% of the photon candidates in the p_T region between 20 and 45 GeV and is also neglected.

The results are compared to next-to-leading order QCD calculations [1] performed using different sets of structure functions [16]. The isolation cut used in the selection of the data suppresses the bremsstrahlung contribution from final state quarks. Such an effect has been taken into account in the QCD calculation [1] by excluding photon–quark configurations with a small angular separation (see Ref. [1] for a description of the exact procedure). The p_T distribution of the data together with the QCD expectations is shown in Fig. 2. The error bars indicate the statistical and p_T dependent systematic uncertainties added in quadrature. The latter arise from the uncertainties in the preshower isolation efficiency and in the Monte Carlo evaluation of ε_γ and ε_π, and from the difference in the energy reconstruction for converted and unconverted photons [5]. The cross–section values are listed in Table 1, where the statistical and the systematic uncertainties are also shown. Not included in Fig. 2 and Table 1 is the overall p_T independent systematic error of 9%, due to the 1% uncertainty on the energy scale (resulting in a 6.4% error on the cross–section), a 5.3% uncertainty on the luminosity measurement, a 2.5% error on the global detection efficiency and a 1% error on the geometrical acceptance. Within these uncertainties and the overall scale error, the data are in fair agreement with the QCD predictions. However, in the low p_T region ($p_T < 30\ GeV$) the measured p_T dependence is significantly steeper than the QCD prediction. Such an effect has also been recently observed by the CDF collaboration at $\sqrt{s} = 1.8\ TeV$ [17]. It could result from the contribution of quark bremsstrahlung which is expected to be important at low p_T. A more accurate theoretical estimate of this contribution is needed for a better quantitative comparison.

5 Double Prompt Photon Production

5.1 Data reduction

The data for this analysis were collected with an electron pair trigger, requiring two electromagnetic clusters in the calorimeter with an azimuthal separation of at least 60^0. The data reduction aims at restricting the analysis to a kinematical region where the trigger efficiency is uniform over the full data taking period, and where the results on single photon identification efficiencies described above can be applied. The events must contain two electromagnetic clusters (γ_1 and γ_2) satisfying the following requirements:

- $p_T\ (\gamma_1) > 10$ GeV and $p_T\ (\gamma_2) > 9$ GeV;
- $|\eta(\gamma_1)| < 0.76$ and $|\eta(\gamma_2)| < 0.76$;
- Z > 0.7 where Z is defined as

$$Z = \ - \ \frac{\overrightarrow{p}_T(\gamma_1) \cdot \overrightarrow{p}_T(\gamma_2)}{|p_T(\gamma_1)|^2}$$

This last cut rejects the events with a large imbalance between the p_T of the two clusters. In this way the contribution from quark bremsstrahlung processes is reduced, as well as the background from jets in which part of the jet energy falls outside the reconstructed cluster.

Photon identification cuts are then applied to each of the two electromagnetic clusters in order to select the final two–photon candidate sample. These criteria are based on the same principles as the ones applied in the single photon analysis; the requirements on track isolation and on the cluster profile are however less strict than in the single photon case, in order to retain a high efficiency for double photon events. The cumulative selection efficiency is measured to be $\varepsilon = 0.725 \pm 0.008$ for each photon. This value does not include the efficiency of the cuts applied to flag a calorimeter cluster as electromagnetic and of the preshower isolation criteria.

The number of candidate events after this selection is 142 .

5.2 Rejection of jet background

In order to estimate the background from γ–jet or two–jet events, the rejection against jets resulting from the photon identification criteria must be known. Such a rejection, ρ, is defined as the probability for a cluster not associated with a direct photon, but recognized as electromagnetic at trigger level, to fulfill the photon identification requirements described in the previous section. It can be evaluated from a sample of electromagnetic clusters using the following set of equations:

$$N_1 = N_j + N_\gamma \qquad [5.1]$$

$$N_2 = \rho N_j + \varepsilon N_\gamma \qquad [5.2]$$

$$\varepsilon N_\gamma = (1-b) N_2 \qquad [5.3]$$

where N_1 is the number of electromagnetic clusters, N_2 is the number of clusters passing the photon identification criteria, and ε is the efficiency of the photon selection defined above. The unknowns are ρ, N_j and N_γ, representing respectively the numbers of jets and direct photons in the initial sample. The variable b, appearing in eq. [5.3] is the background fraction used in the prompt photon analysis (see section 3).

Due to uncertainties in modelling the effect of the SFD angular resolution for two–shower separation in the preshower detector, ε_π and ε_γ are considered fully reliable only for $p_T > 15$ GeV. Therefore ρ was measured directly from equations [5.1]–[5.3] only for $p_T > 16$ GeV, using the high statistics event sample of the single prompt photon analysis. For the lower p_T region ($9 < p_T < 16$ GeV), ρ was evaluated using a sample of single photon candidates extracted from the two–electron trigger, which is fully efficient for $p_T > 9$ GeV. The number of real photons in this sample was evaluated by a Monte Carlo simulation [18] of single prompt photon production, normalized to the measured single prompt photon cross-section in the high p_T bins.

The dependence of ρ as a function of the cluster p_T is shown in Fig. 3, together with the estimated error, which is dominated by the uncertainties on ε_π and ε_γ .

5.3 Background evaluation

In order to evaluate the background content of the double photon candidate sample, the efficiencies and rejection factors can be factorized for the two clusters in the event; one can thus write four equations:

$$N_1 = N_{jj} + N_{\gamma j} + N_{j\gamma} + N_{\gamma\gamma}$$

$$N_2 = \rho_1(1-\rho_2)N_{jj} + \varepsilon(1-\rho_2)N_{\gamma j} + \rho_1(1-\varepsilon)N_{j\gamma} + \varepsilon(1-\varepsilon)N_{\gamma\gamma}$$

$$N_3 = \rho_2(1-\rho_1)N_{jj} + (1-\varepsilon)\rho_2 N_{\gamma j} + \varepsilon(1-\rho_1)N_{j\gamma} + \varepsilon(1-\varepsilon)N_{\gamma\gamma}$$

$$N_4 = \rho_1\rho_2 N_{jj} + \varepsilon\rho_2 N_{\gamma j} + \varepsilon\rho_1 N_{j\gamma} + \varepsilon^2 N_{\gamma\gamma}$$

In these equations N_1 is the original sample where the only requirement on the two clusters is that they satisfy the criteria defining an electromagnetic cluster at trigger level, N_2 is the sample having only the higher p_T cluster identified as a photon, N_3 the sample for which only the lower p_T cluster passes the photon cuts, and N_4 is the double photon candidate sample. The subscripts 1 and 2 on efficiencies and rejections refer to the cluster of higher and lower p_T respectively, while N_{jj} , $N_{\gamma j}$, $N_{j\gamma}$ and $N_{\gamma\gamma}$ are the numbers of jet–jet, single photon and double photon events in the initial sample. Using the known values of ε and ρ, these values can be obtained by solving the system of four linear equations. The calculation is performed dividing the sample in bins of p_T of the higher p_T cluster; for each bin ρ is evaluated at the average p_T value of the first(second) cluster for ρ_1 (ρ_2) respectively.

The numbers N_{1-4} together with $N_{\gamma\gamma}$ and its error are shown in Table 2 for four p_T bins.

Table 2: Numbers of events used for background evaluation (N_1 to N_4) and number of real double photon events ($\varepsilon^2 N_{\gamma\gamma}$)

Δp_T (GeV)	N_1	N_2	N_3	N_4	$\varepsilon^2 N_{\gamma\gamma}$
$10-12$	2585	296	298	68	29.7 ± 8.9
$12-18$	3548	400	358	58	17.0 ± 9.1
$18-24$	704	79	48	12	8.1 ± 3.6
$24-31$	254	24	9	4	3.4 ± 2.0

The values of the unknowns, summed over all p_T bins are : $N_{jj} = 6020.9$, $(N_{\gamma j} + N_{j\gamma}) = 959.4$ and $N_{\gamma\gamma} = 110.7$. The dominant error on $N_{\gamma\gamma}$ is the statistical error on the number of candidates. From the number $N_{\gamma\gamma}$ in each bin and the corresponding errors, calculated including all the relevant p_T dependent contibutions, the $\gamma\gamma$ signal turns out to be 58.2 ± 13.4 events, with a statistical significance of 4.3 standard deviations.

5.4 Cross–section calculation and comparison with QCD

Values of the cross–section for double prompt photon production, $d\sigma_{\gamma\gamma}/dp_T$, are obtained from the number of photons falling inside a given p_T bin when the event contains a second photon. With this definition, each event is counted twice: once for each p_T bin to which the two photons belong. The formula for the cross–section is:

$$\frac{d\sigma_{\gamma\gamma}}{dp_T} = \frac{N^*_{\gamma\gamma}}{\varepsilon_C^2\ A(p_T)\ \Delta p_T\ \mathcal{L}}$$

where $N^*_{\gamma\gamma}$ is the number of photons in each bin, ε_C is the efficiency of the cuts defining an electromagnetic cluster, $A(p_T\ )$ is the geometrical acceptance, Δp_T is the bin size and $\mathcal{L}$ is the integrated luminosity.

The geometrical acceptance $A(p_T\ )$ is obtained by means of a Monte Carlo simulation which used a generator of double prompt photon events to lowest order [18], and takes into account the effect of the spread of the interaction vertex as well as the rapidity boundary $\mid \eta \mid < 0.76$ applied to both photon candidates in the data.

Table 3: Double prompt photon differential cross section.

$\Delta p_T\ (GeV)$	$p_T(GeV)$	$d\sigma/dp_T(pb/GeV)$
$10 - 12$	10.9	4.31 ± 1.03
$12 - 18$	14.1	0.922 ± 0.33
$18 - 24$	20.4	0.346 ± 0.125
$24 - 31$	26.9	0.116 ± 0.063

The cross–section values so obtained are given in Table 3 and shown in Fig. 4. The quoted errors include the statistical and all p_T –dependent systematic uncertainties. In addition, there is a normalization uncertainty of 6.8 % which is obtained by adding in quadrature the following errors:

- the 5.3 % error on the luminosity;
- a 3.5 % error resulting from a 1 % uncertainty on the photon energy scale;
- a 2.4 % error resulting from the 1.1 % uncertainty which affects the determination of ε_C.

Fig. 4 also shows the results of two independent QCD predictions to next–to–leading order (NLO). The calculation of Ref. [2] is performed analytically, whereas a Monte Carlo method is used for Ref. [3]. In the two cases the same parameters are used, namely: a NLO definition of α_s; the HMRSB structure functions [19] ; $Q^2 = p_T^2$; and no isolation criteria on the photon. However, while the calculation of Ref. [3] is performed by requiring $\mid \eta \mid < 0.76$ for both photons, as in the data, in the analytical calculation of Ref. [2] this requirement is applied to only one photon, resulting in a cross–section which

is larger by approximately a factor of 2.5. The result of this calculation was therefore corrected for the reduced acceptance of the data using the Monte Carlo simulation described above. For both predictions the agreement is good apart from the first bin in p_T where the data lie significantly above the theoretical prediction. This discrepancy could be due to the theoretical uncertainties in the calculation of the diagrams where the final state photons are radiated from quarks (bremsstrahlung diagrams), which contribute mostly to the lowest p_T bin. The earlier measurement [20] of the two photon cross-section, performed in π^-p interactions at $\sqrt{s} = 23\ GeV$, is in good agreement with QCD predictions. However, that analysis covers a different region in $x_T = 2p_T/\sqrt{s}$, where double prompt photon production is dominated by the annihilation diagram $q\overline{q} \rightarrow \gamma\gamma$.

Acknowledgements

We thank P. Aurenche and collaborators for providing the theoretical predictions relevant to the experimental conditions of the present study in the form of a computer programme. We also thank J. Owens and collaborators for providing the result of their recent calculation of double prompt photon production in a form directly comparable to the experimental data.

The technical staff of the institutes collaborating in UA2 have contributed substantially to the construction and operation of the experiment. We thank them deeply for their continuous support. The experiment would not have been possible without the very successful operation of the improved CERN $\overline{\text{p}}$p Collider, whose staff and coordinators we sincerely thank for their collective effort. Financial support from the Schweizerischen Nationalfonds zur Förderung der Wissenschaftlichen Forschung to the Bern group, from the UK Science and Engineering Research Council to the Cambridge group, from the Bundesministerium für Forschung und Technologie to the Dortmund and Heidelberg groups, from the Australian Research Council, the CRA Pty Ltd, and the Victorian Education Foundation to the Melbourne group, from the Institut National de Physique Nucléaire et de Physique des Particules to the Orsay group, from the Istituto Nazionale di Fisica Nucleare to the Milano, Pavia, Perugia and Pisa groups and from the Institut de Recherche Fondamentale (CEA) to the Saclay group are acknowledged.

References

[1] P. Aurenche et al.: Phys Lett. **B140** (1984) 87;
P. Aurenche et al.: Nucl. Phys. **B297** (1988) 661;
P. Aurenche et al.: Phys. Rev. **D42** (1990) 1440.

[2] P. Aurenche et al.: Z. Phys. **C29** (1985) 459.

[3] B. Bailey, J. Ohnemus, and J.F. Owens, FSUHEP-920320 and DTP/92/18.

[4] UA2 Collaboration, J.A. Appel et al.: Phys. Lett. **B176** (1986) 239;
UA2 Collaboration, R. Ansari et al.: Z. Phys. **C41** (1988) 395;
UA1 Collaboration, C. Albajar et al.: Phys. Lett. **B209** (1988) 385.

[5] UA2 Collaboration, J. Alitti et al.: Phys. Lett. **B263** (1991) 544.

[6] UA2 Collaboration, C.N. Booth, Proc. 6th Topical Workshop on Proton–Antiproton Collider Physics (Aachen, 1986), eds. K. Eggert et al. (World Scientific, Singapore, 1987) p. 381.

[7] A. Beer et al.: Nucl. Instrum. Methods **A224** (1984) 360.

[8] R. Ansari et al.: Nucl. Instrum. Methods **A279** (1989) 388.

[9] F. Bosi et al.: Nucl. Instrum. Methods **A283** (1989) 532.

[10] R. Ansari et al.: Nucl. Instrum. Methods **A263** (1988) 51.

[11] R.E. Ansorge et al.: Nucl. Instrum. Methods **A265** (1988) 33;
J. Alitti et al.: Nucl. Instrum. Methods **A279** (1989) 364.

[12] K. Borer et al.: Nucl. Instrum. Methods **A286** (1990) 128.

[13] R. Ford and W. Nelson, SLAC–210 (1978).

[14] UA2 Collaboration, M. Banner et al.: Z. Phys. **C27** (1985) 329.

[15] G. Blaylock et al.: Proc. Itern. Conf. on the Impact of Digital Microelectronics and Microprocessors on Particle Physics, eds. M. Budinich et al. (World Scientific, Singapore, 1988) 247;
P. Baehler at al., ibid., 254.

[16] D.W. Duke and J.F. Owens, Phys. Rev. **D30** (1984) 49;
E. Eichten et al.: Rev. Mod. Phys. **56** (1984) 579;
erratum Rev. Mod. Phys. **58** (1986) 1065;
P. Aurenche et al.: Phys. Rev. **D39** (1989) 3275.

[17] CDF Collaboration, F. Abe et al.: Phys. Rev. Lett. **68** (1992) 2734.

[18] H.U. Bengtsson and T. Sjöstrand, PYTHIA, Comput. Phys. Commun. **46** (1987) 43.

[19] P.N. Harriman, A.D. Martin, R.G. Roberts, and W.J. Stirling, Phys. Rev. **D42** (1990);
Phys. Lett. **B243** (1990) 421.

[20] E. Bonvin et al.: Z. Phys. **C41** (1989) 591.

Figure captions

Fig. 1a Conversion fraction for photon candidates as a function of the cluster energy. The curves labeled ε_γ and ε_π are the conversion probabilities for single photons and multiphoton background, respectively.

Fig. 1b The fractional multiphoton background contamination in the sample of photon candidate events as a function of the reconstructed photon p_T.

Fig. 2 The invariant differential cross–section for direct photon production is compared with the next–to–leading order QCD calculation of Ref. [1] with two different sets of structure functions [16]: Duke–Owens set 1 (DO1); and Aurenche et al. (ABFOW) with an optimized Q^2 scale (OPT) and $Q^2 = p_T^2$. The errors shown include statistical and p_T dependent systematic errors added in quadrature.

Fig. 3 Probability ρ for electromagnetic clusters not generated by a direct photon to pass the photon identification cuts, as a function of the cluster p_T .

Fig. 4 Differential double prompt photon cross-section . The error bars include the statistical error and the p_T -dependent systematics. The superimposed curves are the NLO QCD calculations of Ref. [2] (dashed line) and of Ref. [3] (full line).

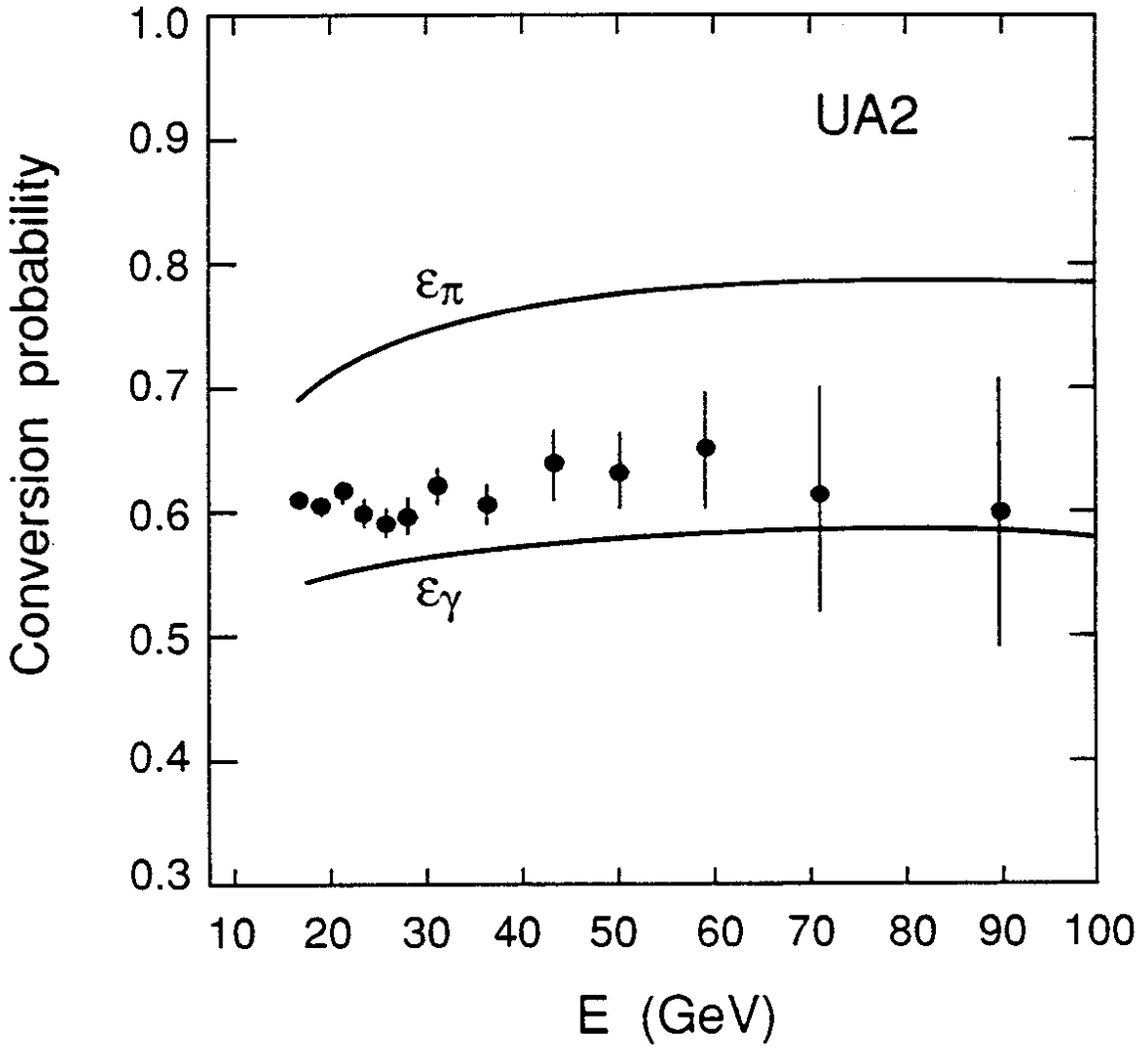
UA2
Conversion probability
E (GeV)
ε_π
ε_γ
1.0
0.9
0.8
0.7
0.6
0.5
0.4
0.3
10
20
30
40
50
60
70
80
90
100

Figure 1a

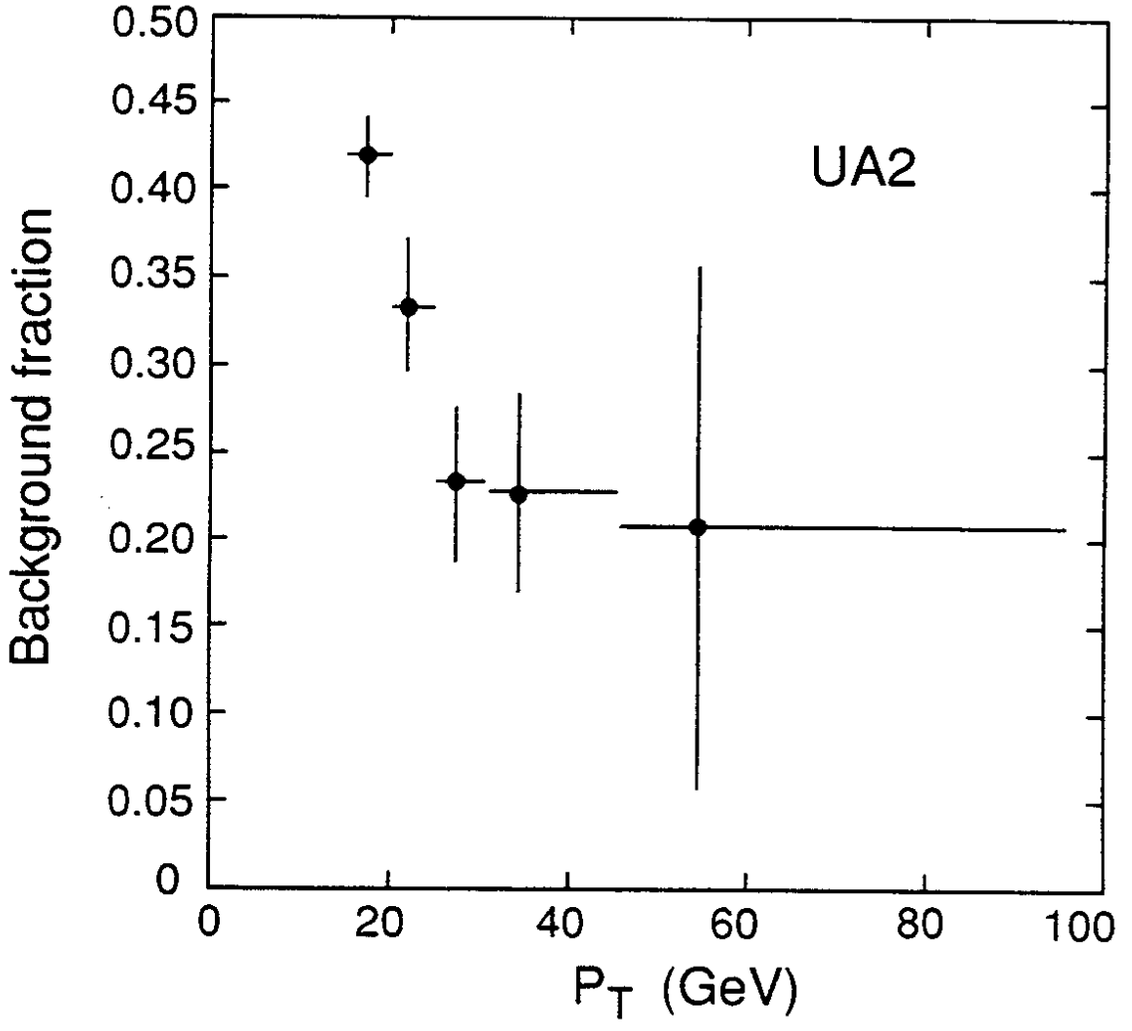
Background fraction
0.50
0.45
0.40
0.35
0.30
0.25
0.20
0.15
0.10
0.05
0
UA2
0
20
40
60
80
100
P_T (GeV)

Figure 1b

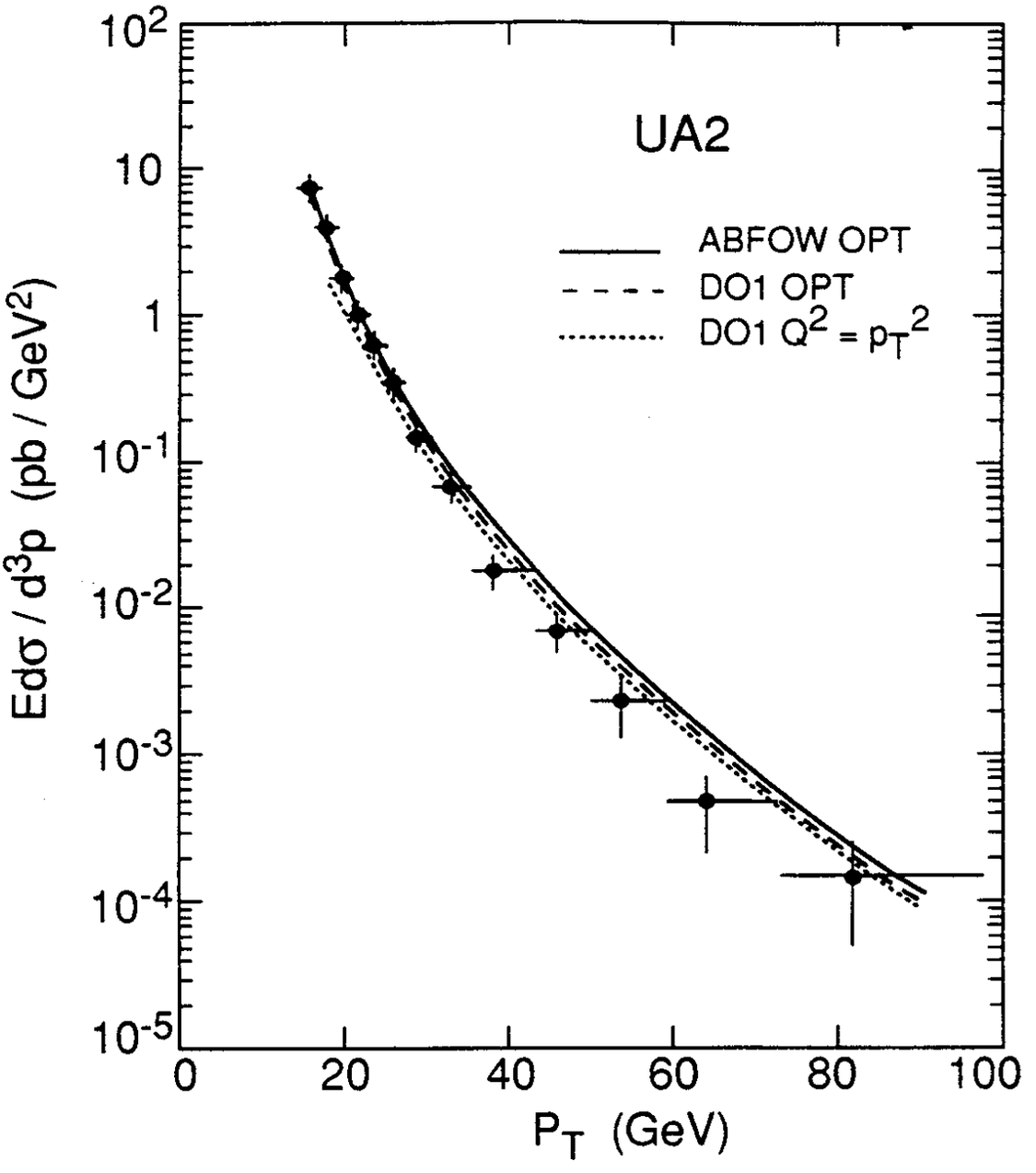
UA2
ABFOW OPT
DO1 OPT
DO1 $Q^2 = p_T^2$
$Ed\sigma / d^3p$ (pb / GeV^2)
P_T (GeV)
10^2
10
1
10^{-1}
10^{-2}
10^{-3}
10^{-4}
10^{-5}
0
20
40
60
80
100

Figure 2

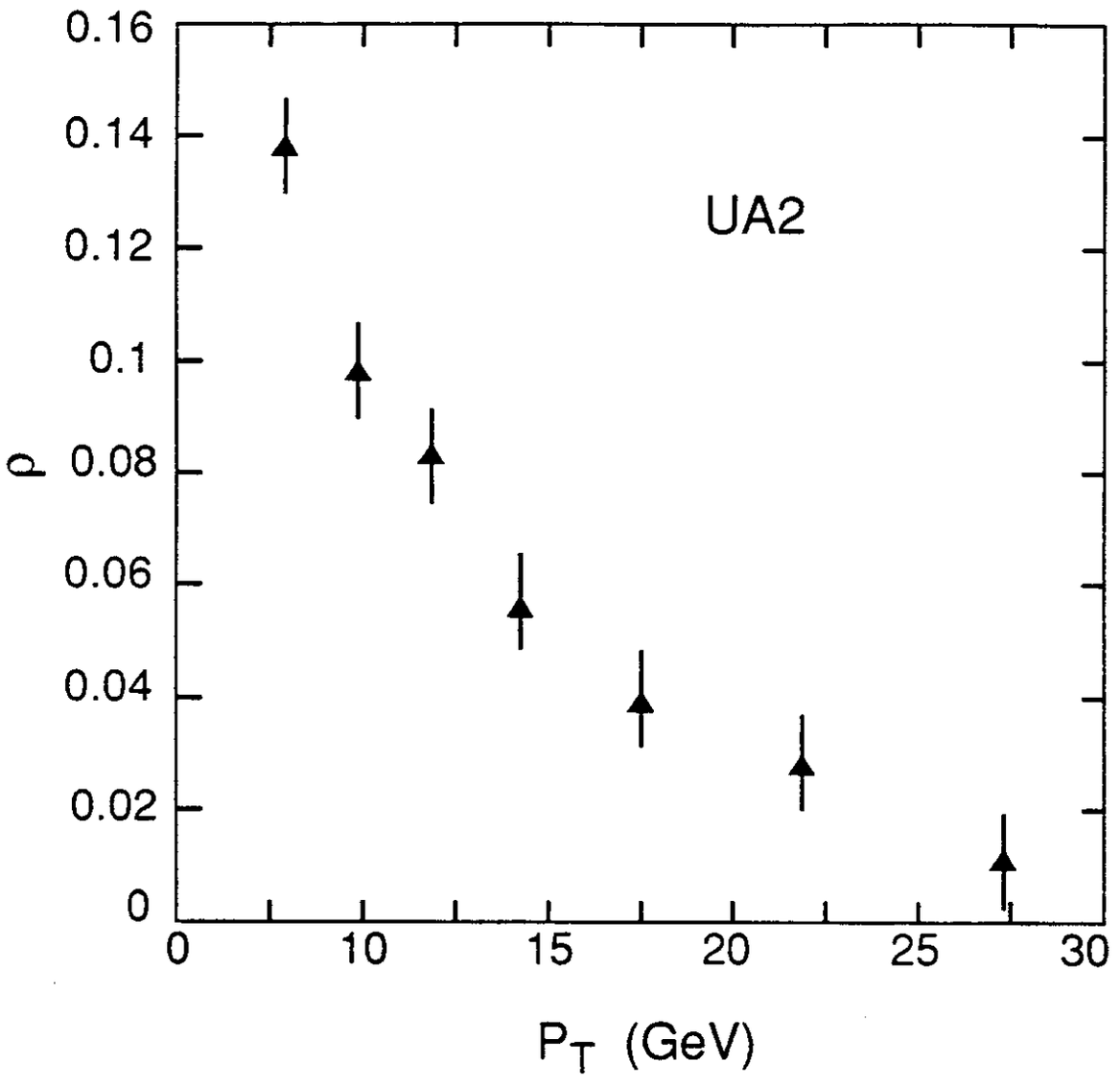

Figure 3

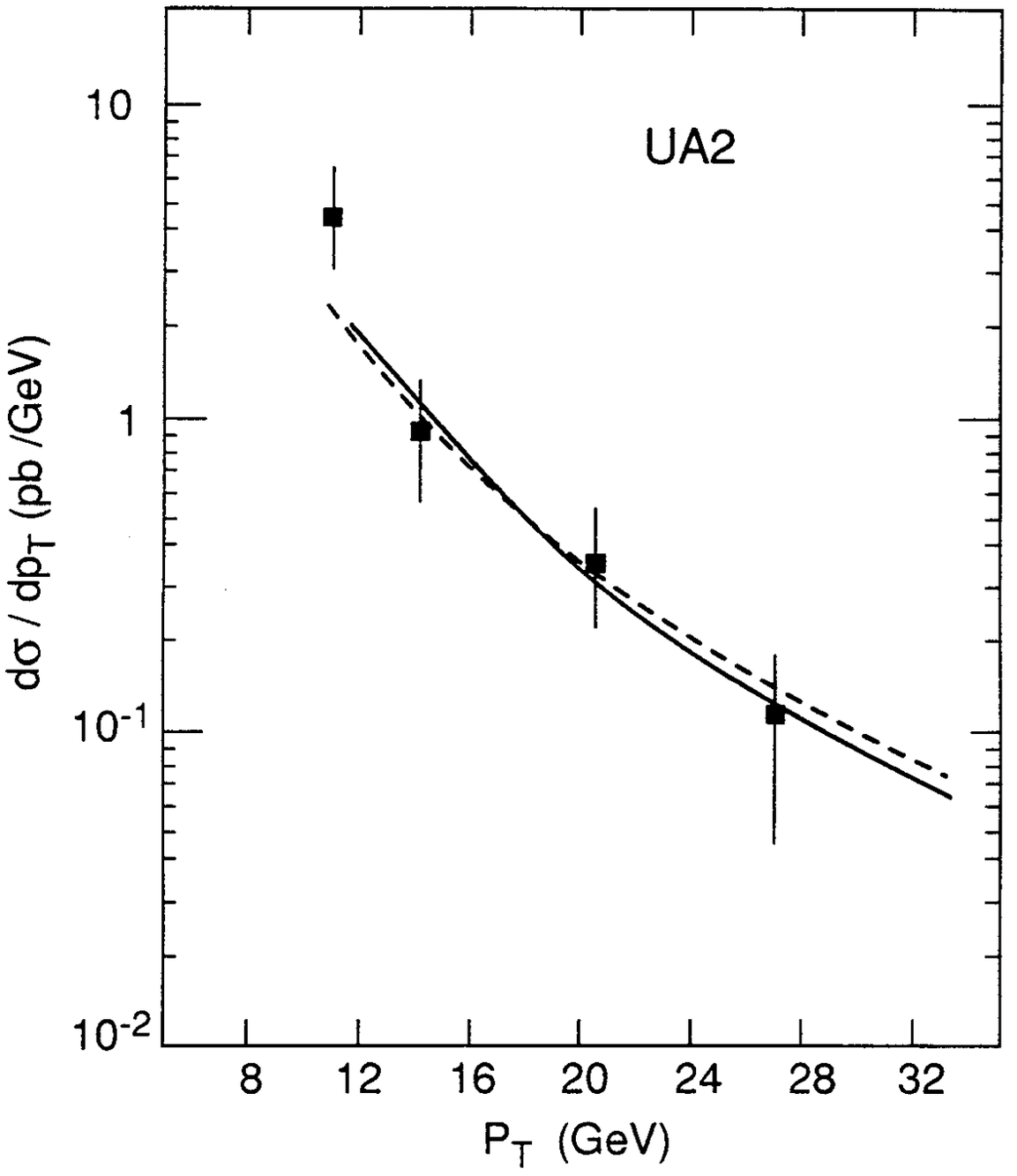

Figure 4